








Physical-Chemical Effects of Nanoparticles on Electropolymerized Polyaniline

José Agenor Carvalho Júnior¹, Ana Paula Moreira Barboza¹ , Giovanna Machado² , Bernardo R. A. Neves³ , Alan B. de Oliveira¹ , Ronaldo J. C. Batista¹ , Fernando Gabriel S. Araújo¹, Jaqueline S. Soares¹ , Taise M. Manhobosco^{1,*} 

¹ Departamento de Física, Universidade Federal de Ouro Preto, Campus Universitário Morro do Cruzeiro/ICEB/DEFIS, 35400-000, Ouro Preto, Minas Gerais, Brazil

² Centro de Tecnologias Estratégicas do Nordeste – CETENE, Av. Prof. Luiz Freire, 01, 50740-540, Recife, Brazil

³ Departamento de Física, ICEx, Universidade Federal de Minas Gerais, 31270-901, Belo Horizonte, MG, Brazil

* Correspondence: taise@ufop.edu.br

Scopus Author ID 127884506000

Received: 5.08.2021; Revised: 24.09.2021; Accepted: 27.09.2021; Published: 2.11.2021

Abstract: The incorporation of nanoparticles on polymer films is possible to obtain materials with desired properties. In the present work, we address the physical-chemical influence of nanoparticles in polymer films by producing and characterizing polyaniline hybrids with SiO₂ and Au nanoparticles and comparing them with films with TiO₂ nanoparticles. The hybrid films were characterized by SEM, EDS, UV-Vis, AFM, Raman, and cyclic voltammetry. Unlike TiO₂ nanoparticles, SiO₂ and Au nanoparticles do not promote any noticeable change in polyaniline oxidation state in less acid environments (pH 5.9 and 6.15). However, in those environments, the presence of nanoparticles significantly increases the film's conductivity. At a pH of 1.5 and 3.9, all three kinds of nanoparticles are screened by ions from the solution diminishing their physical-chemical effects on polyaniline. Thus, our results suggest that, in general, nanoparticles don't have any physical-chemical effects on polyaniline films when deposited in acid enough environments but can change their physical and chemical properties when deposited in less acid environments.

Keywords: polyaniline; nanoparticles; electrochemistry; AFM; Raman.

© 2021 by the authors. This article is an open-access article distributed under the terms and conditions of the Creative Commons Attribution (CC BY) license (<https://creativecommons.org/licenses/by/4.0/>).

1. Introduction

Polyaniline (PANI) is a conductive polymer with a differentiated doping mechanism that occurs by protonation, whereas in other polymers, such as intrinsically conducting polymers, it occurs by oxidation or reduction [1-3]. Besides, PANI exhibits good stability in the air in doped and undoped states [4,5]. Another important advantage of PANI over other conductive polymers is the ease of film synthesis and processing. For these reasons, this material has great potential for several applications, especially in the electronic area [6-24]. For example, studies on applying polyaniline in low-cost photovoltaic organic cells have been previously reported [25,26].

Furthermore, the incorporation of nanoparticles in polyaniline films could be a way to improve desired properties, such as conductivity, leading to new materials and technology. For instance, hybrids of PANI and gold nanoparticles were used as biosensors to detect glucose levels [27,28]. In another work, hybrid films of polyaniline and titanium dioxide nanoparticles were used to coat aluminum alloys, presenting lower current density (two orders of magnitude)

than nanoparticle-free films. Therefore, aluminum alloy showed an increase in corrosion resistance [29]. The literature also reports incorporating silver nanoparticles in polyaniline, which promotes improvement in electrical conductivity compared to pure PANI [30].

Electrodeposition is a cheap and versatile technique that allows the production of a wide variety of films and coatings [31-34], including films incorporating nanostructured materials [35,36]. A few years ago, some of the authors [36] reported the production of hybrids of titanium dioxide nanoparticles and PANI films using pulsed electrodeposition at different pHs (at pH 1.5, 3.9, and 5.9). At pH 5.9, the TiO₂ nanoparticles significantly influence film characteristics; for instance, the current density of PANI films increases in one order of magnitude because of the TiO₂ incorporation of nanoparticles. On the other hand, at low pH (1.5), nanoparticles have negligible effects on all observed film properties. The observed differences in the effects of nanoparticles on films deposited at low and high pH were ascribed to the screening of the charged TiO₂ nanoparticles by opposing sign ions in the low pH solution. Such a screening mechanism prevents the physical contact between nanoparticles and polyaniline monomers and, therefore, diminishes the physical effects (such as charge transfer and formation of PANI/nanoparticle heterojunctions) and chemical effects (such as changes in PANI oxidation states) of nanoparticles on PANI films at low pH. Thus, the following question arises: how specific for TiO₂ nanoparticles is the behavior described above? In other words, can the observed behavior, at least in part, be generalized to any other nanoparticles? To answer this question, we have performed further studies on the influence of SiO₂ and Au nanoparticles when incorporated in PANI films. The referred nanoparticles were incorporated into electrodeposited polyaniline films at different pH (1.5, 3.9, 5.9, and 6.15). Morphological, optical, and electrical properties were investigated, and the results are explained in terms of physical and chemical interactions.

2. Materials and Methods

2.1. Deposition of PANI films.

PANI films were pulsed electrodeposited on an indium-tin-oxide (ITO – Delta Technologies Corporation) glass substrate (specific resistance: 4-8 W/square). ITO glass substrates were cleaned with detergent (Aquet – Bel Art), acetone, alcohol, and bidistilled water, respectively. A final cleaning procedure included the immersion of the substrates in a 20% v/v ethanalamine solution at 80 °C for 20 minutes and washed with bidistilled water. During the cleaning procedure, the substrates were dried with nitrogen gas.

The electrodeposition setup and conditions were performed as described previously by our group [36]. In brief, the pulsed depositions were carried out at 1.1 VSCE for 15 min and a pulse frequency of 0.1 Hz. Electrodeposition solutions were composed of aniline (0.1 M; Sigma Aldrich) and H₂SO₄. The pH of the electrodeposition solution was adjusted by dropping H₂SO₄ in the solution until the desired pH was reached. To produce PANI/SiO₂ hybrid films, SiO₂ nanoparticles (Sigma Aldrich, Mw = 60.08 g mol⁻¹, particle size 10-20 nm) were added to electrodeposition solution with a concentration of 0.025 M at different pH. In addition, our group synthesized gold nanoparticles at pH 6.15 were added to electrodeposition solution to produce PANI/Au hybrid films.

2.2. *Synthesis of Au NPs.*

Citrate-stabilized gold nanoparticles (Au NPs) with the size of around 10 nm have been synthesized. The excess of sodium citrate during nucleation with tannic acid has to play a leading role in forming a high number (7×10^{13} NP/mL) of small seeds with a very narrow distribution. We use this method to obtain Au NPs with good control sizes around 6-10 nm with versatile syntheses conditions, allowing studying the optical properties of nanoparticles in this size regime.

The synthesis method was obtained using Piella synthesis with some modifications [37]. Briefly, the synthesis was performed by injecting 1 mL of HAuCl₄ (25 mM) into a mixed solution of 0.1 mL of tannic acid (2.5 mM) containing 150 mL of sodium citrate (2.2 mM) at 70 °C. The solution changes from light yellow to red-violet, indicating the formation of Au NPs.

2.3. *Characterization of PANI films.*

2.3.1. Scanning electron microscopy and energy dispersive spectroscopy characterization.

Scanning Electron Microscopy (SEM) images and energy dispersive spectroscopy (EDS) analysis was carried out in a Vega3 Tescan at an acceleration voltage of 25 kV. The conductivity of the PANI films was ensured by the deposition of gold conducting coatings.

2.3.2. Optical absorption spectra characterizations.

Optical absorption spectra were acquired using a UV-1800 (SHIMADZU) spectrophotometer over a 190-1100 nm wavelength range.

2.3.3. Atomic force microscopy characterization (AFM).

To AFM characterization, we used a Bruker MultiMode 8 SPM, in the intermittent contact-imaging mode. Si cantilevers (from Nanosensors), with spring constants of 10 – 130 N/m and a tip radius of curvature ~10 nm, were employed throughout the study for sample imaging.

2.3.4. Raman spectroscopy characterization.

Raman spectra were recorded with WITec's Raman microscope alpha300 with the excitation wavelength of 532 nm. The laser power was kept at 0.5 mW.

2.3.5. Electrochemical characterization.

Cyclic voltammetry curves of films electropolymerized at different pH, for instance, pH 1.5, 3.9, 5.9, and 6.15, were performed to evaluate the films' electrochemical behavior. Experiments were performed in a 0.1 M H₂SO₄ solution to compare the electrochemical activity of film obtained at different pHs. The potential was cycled between -0.4 VSCE and 0.8 VSCE at a scan rate of 0.01 V/s by using a PGSTAT 128N potentiostat/galvanostat (Metrohm-Autolab).

3. Results

3.1. SEM and EDS.

It is possible to view larger clumps in PANI films deposited at pH 1.5 (Figure 1 (a)) when compared to films at pH 3.9 and 5.9 (Figure 1 (b)) and Figure 1 (c), respectively). Probably, such larger clumps are due to the larger amount of deposit, which is consistent with visual observations and AFM measurements that show greater amounts of deposited polyaniline as the pH becomes more acid. The morphology of the PANI films at pH 3.9 (Fig. 1 (b)) reveals that small clumps covered the surface, and the morphology of PANI films deposited at pH 5.9 (Figure 1 (c)) shows irregularly shaped clumps. The influence of pH can be observed through the morphology of the films; however, SEM images do not provide evidence of the presence of SiO₂ and Au nanoparticles due to technique resolution, as has been previously reported by our group [36].

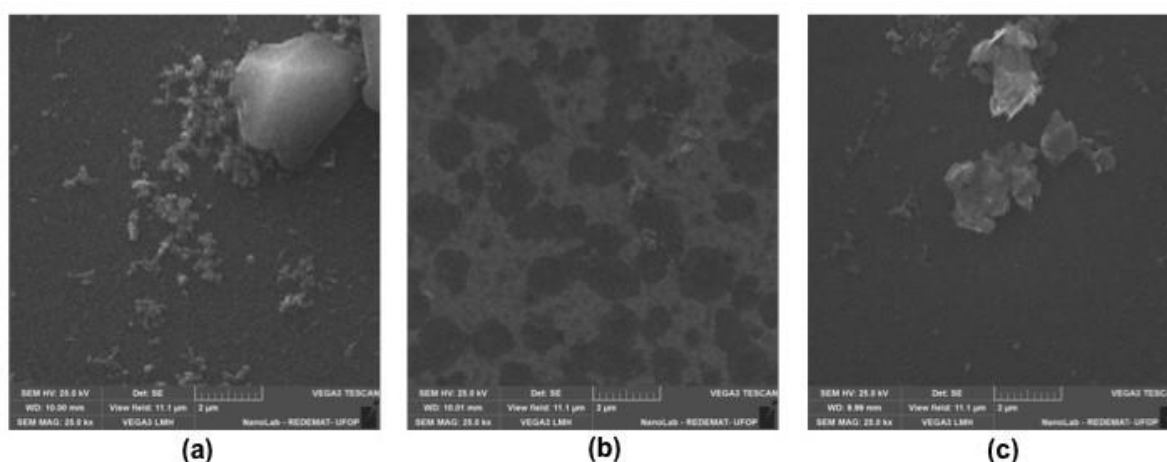


Figure 1. SEM image of PANI films obtained at different pH: (a) 1.5; (b) 3.9; (c) 5.9.

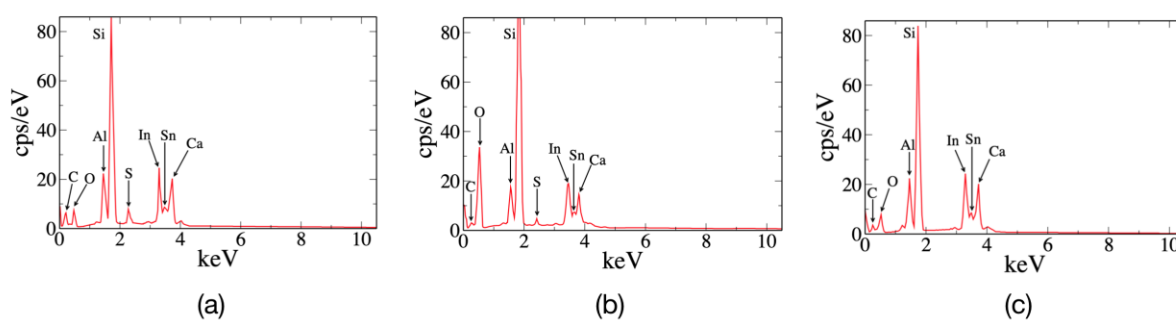


Figure 2. EDS spectra of PANI/SiO₂ hybrid films deposited at different pH: (a) 1.5; (b) 3.9; (c) 5.9.

Let us now discuss the composition of films with nanoparticles incorporation deposited at different pHs. Figure 2 shows the composition of the PANI films with SiO₂ nanoparticles plus the composition of the substrate, which is composed of an indium tin oxide (ITO) coating onto the glass. Besides being responsible for the large Si peak, the used glass is also responsible for the Al and, Ca peaks shown in all panels; Al is used as a stabilizer, and Ca is used to decrease the glass melting point. The most remarkable characteristics of those spectra, however, are the presence of a noticeable S peak in panel (a), a less intense S peak in panel (b), and the absence of S in panel (c). The only possible source of S atoms is the SO₄²⁻ anions originated from the electrolyte solution and, as will be further discussed in the text, such a

result gives strong support to the hypothesis that nanoparticles become charged and screened by opposing sign ions from electrolyte before being incorporated into the PANI film.

3.2. UV-Vis spectroscopy.

The UV-Vis spectrum of PANI is greatly dependent on the oxidation state. In order to verify the effects of nanoparticles and pH on the oxidation state of PANI films, we have also performed UV-Vis spectroscopy characterization. Figure 3 exhibits the absorption spectra of the PANI films with and without incorporation of (a) SiO₂ nanoparticles at pH 1.5, 3.9, and 5.9 and (b) Au nanoparticles at pH 6.15.

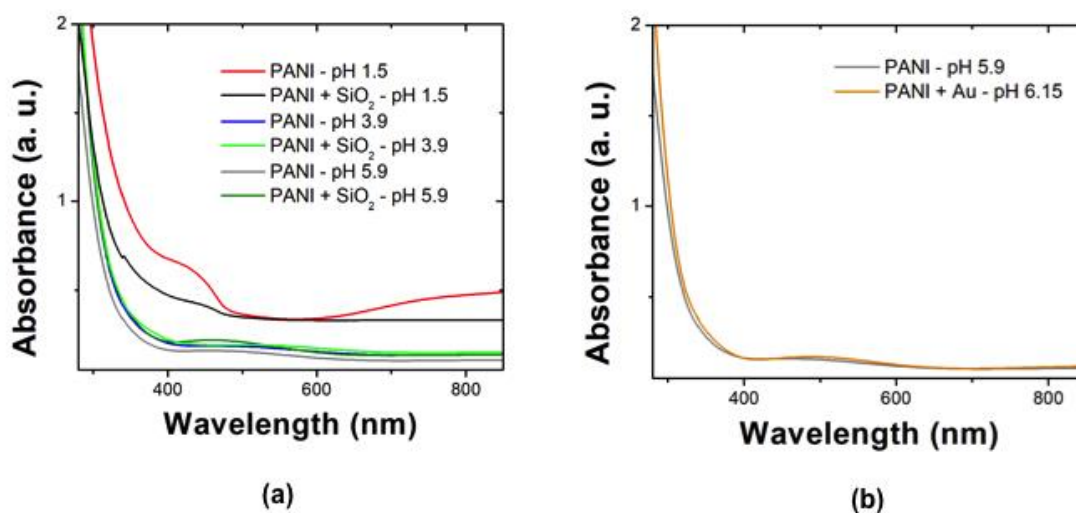


Figure 3. UV-Vis absorption spectra of PANI films with and without incorporation of ((a) SiO₂ and (b) Au) nanoparticles deposited at different pH.

Films electrodeposited at pH 1.5 (Figure 3 (a)) show a distorted absorption band between 300 nm and 450 nm. The overlap of two peaks explains such distortion, one occurs around 300 nm, which may be related to the π - π^* transition in the benzene ring structure [38-43]; and another one between 410-440 nm, which is related to the polaron- π^* transition [36,44-49]. It also exhibits an absorption band between 650-800 nm, which can be attributed to the π -polaron transition [36,40-43]. According to the literature, the oxidation state of PANI film obtained at more acid electrodeposition solutions (pH 1.5) is emeraldine salt (doped state) [33,36,40,41].

Films electrodeposited at pH 3.9 (Fig. 3 (a)) have two bands, one around 368 nm and one approximately 575 nm, which are assigned to the π - π^* transition [44,50,51] and Pierls transition [41,44,52], respectively. According to the literature, the oxidation state of PANI film obtained at pH 3.9 is the pernigraniline form of PANI (oxidized form) [38,41,47]. The same optical behavior is observed for PANI films electropolymerized at pH 5.9 (Figure 3 (a)). Similar results were previously reported by our group [36].

The addition of SiO₂ nanoparticles to PANI at different pH (see Figure 3 (a)) does not promote any significant changes in polyaniline's optical properties or oxidation state. The same happens for Au nanoparticles incorporated at a pH of 6.15 (see Figure 3 (b)). According to the literature, films produced at lower pH, like pH 1.5, are composed of emeraldine, while films at higher pH (3.9, 5.9, and 6.15) are composed of pernigraniline form PANI [38,41,47]. Therefore, it is found that neither gold nanoparticles nor silicon dioxide nanoparticles, no matter the electrodeposition solution pH, cause changes in the polyaniline oxidation state. In particular, it has been shown [36] that incorporating TiO₂ nanoparticles in PANI films at pH

5.9 changes the oxidation state of the polymer. Films electrodeposited at pH 5.9 were composed of pernigraniline, while the addition of TiO₂ promotes an expressive change in the oxidation state of PANI, turning it to a doped state (emeraldine). Such results are confirmed by means of Raman measurements, and further discussion will be made elsewhere in the text.

3.3. Raman spectroscopy.

For the sake of comparison and completeness, we also performed Raman spectroscopy characterization on PANI films deposited at different pHs (1.5, 3.9, 5.9, and 6.15) with and without SiO₂ and Au nanoparticles incorporation. Figure 4 shows representative Raman spectra acquired from the same films discussed earlier. Spectra in Figure 4 were taken from PANI films with and without incorporation of SiO₂ nanoparticles at pH 1.5 (Figure 4 (a)), pH 3.9 (Figure 4 (b)), and pH 5.9 (Figure 4 (c)), as well as those from PANI films with the incorporation of Au nanoparticles at pH 6.15 (Figure 4 (c)). Spectra obtained in different regions of PANI films showed the same spectral signatures, indicating homogeneity in the electrodeposited films. This behavior was observed for all the PANI films produced in this work.

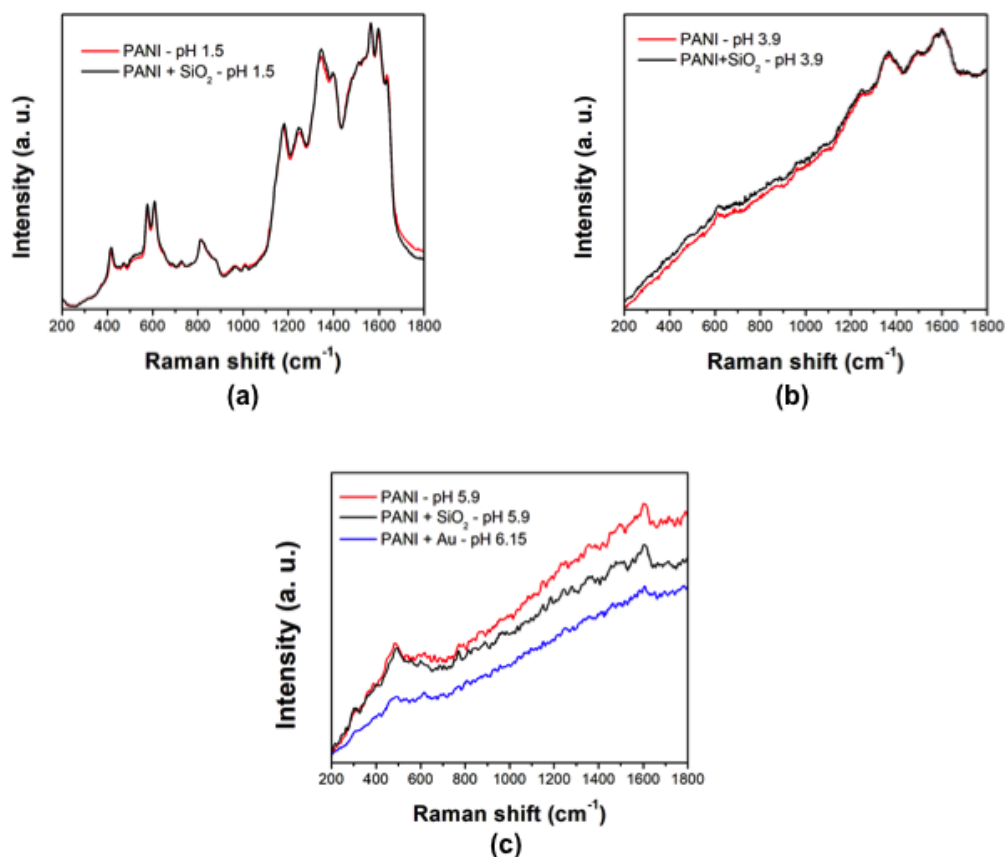


Figure 4. Raman spectra of PANI films electrodeposited at different pH with and without incorporation of SiO₂ and Au nanoparticles. Representative Raman spectra acquired from PANI films: (a) pH 1.5 without and with SiO₂. (b) pH 3.9 without and with SiO₂. (c) pH 5.9 without and with SiO₂, and pH 6.15 with Au. The peak at 482 cm⁻¹ in panel (c) came from ITO glass, and the other peaks are described in Table 1.

Analysis of the spectral features in Figures 4 (a), (b), and (c) show no noticeable effect of the nanoparticles on the molecular structure of PANI films, so as observed with UV-Vis measurements. Raman spectroscopy indicates that depositions at pH 1.5 (Fig. 4 (a)) may produce films composed of emeraldine, while depositions at pH 3.9 and 5.9 may produce films

composed of pernigraniline (Fig. 4 (b) and (c)), these aspects of Raman spectroscopy confirms UV-Vis results. Table 1 presents all Raman bands and their assignments so as observed in Fig. 4. As mentioned earlier, PANI films electrodeposited at pH 1.5 and 3.9 with and without incorporating SiO₂ nanoparticles have similar chemical characteristics. The same is valid for PANI films deposited at pH 5.9 and 6.15, with SiO₂ and Au nanoparticles, respectively, which contrasts with previous Raman results obtained by our group for TiO₂ nanoparticles at pH 5.9. In that case, the incorporation of TiO₂ nanoparticles greatly influences the oxidation state of PANI.

Table 1. Assignment of Raman bands.

Wavelength (cm ⁻¹)			Assignments	Reference
pH 1.5	pH 3.9	pH 5.9		
417	-	-	Out of plane ring deformations	36
576	-	-	Ring deformation	36
607	-	-	Ring deformation	36
-	612	-	C-H deformation of the quinoid ring	53
814	-	-	Amine deformation	36
1180	-	-	C-H bending of the quinoid ring	36
1254	1249	-	C-N stretching in polaronic units	54
1343	-	-	C-N ⁺ stretching vibrations	36
-	1350	-	C-N stretching in polaronic units	54, 55
-	1368	-	C-N stretching in polaronic units	54, 55
-	1493	-	C=N vibrations	56
1564	-	-	C-C stretching of structures intermediate between quinoid and semiquinoid structures	36
-	1574	-	C=C stretching in benzene and quinoid rings	57
1596	-	-	C-C stretching modes of semiquinoid units	36
-	1601	-	C-C stretching in benzene ring	53
-	-	1606	quinone diimine units	36, 58
1635	-	-	phenazine, phenoxazine, safranine like segments	36

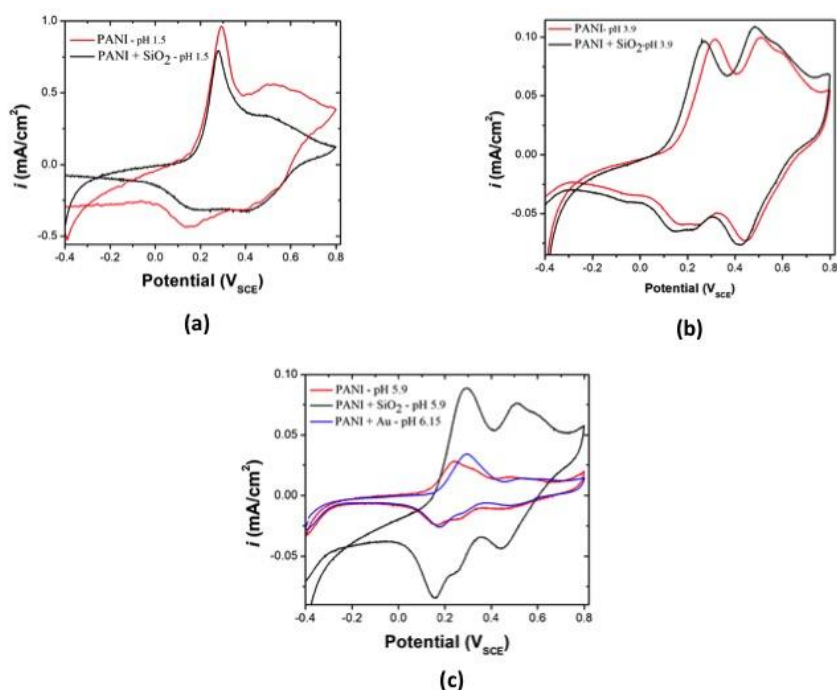


Figure 5. Cyclic voltammetry curves of pristine and hybrid PANI films in 0.1 M H₂SO₄. (a) PANI films deposited at pH 1.5 with and without SiO₂ nanoparticles; (b) PANI films deposited at pH 3.9 with and without SiO₂ nanoparticles; (c) PANI films deposited at pH 5.9 with and without SiO₂ nanoparticles and at pH 6.15 with gold nanoparticles. A scanning rate of 0.01 V/s.

3.4. Cyclic voltammetry.

Cyclic voltammetry of PANI films electrodeposited at pH 1.5, 3.9, and 5.9 with and without SiO₂ incorporation and at pH 6.15 with Au incorporation are presented in Fig. 5. It can be observed that, in all tested cases, the cyclic voltammetry curves present four redox processes corresponding to oxidation and reduction of PANI [36].

The pH effect is well observed, and it is in good agreement with UV-Vis and Raman results; that is, the electropolymerization performed in more acid solutions (pH 1.5) produces PANI in an emeraldine state (conducting form) with currents reaching up to 1 mA/cm². By increasing the pH of electrodeposition solution to 3.9, 5.9, and 6.15, the pernigraniline form of PANI (non-conducting form) is produced, and a decrease in the current density of cyclic voltammograms is observed as expected for PANI of lower conductivity as pernigraniline.

The effect of SiO₂ nanoparticles on morphology and oxidation state of films deposited at pH 1.5 is negligible, as in the case of PANI with TiO₂ nanoparticles at the same conditions [36]. However, a decrease of 18% in the value of maximum current density is observed, which will be discussed in detail next.

At a pH of 3.9, only small changes in cyclic voltammetry are observed, which indicates that the screening of SiO₂ nanoparticles still plays a fundamental role (see Figure 5 (b)) in PANI films with nanoparticles incorporation. However, at pH of 5.9 and 6.15, the effect of nanoparticles in voltammetry curves (Figure 5 (c)) is clear. Cyclic voltammetry curves show an increase in current density due to the presence of SiO₂ and Au nanoparticles.

Table 2. Film thickness obtained from AFM measurements and current density developed in cyclic voltammetry tests for different electrodeposition pH with and without nanoparticles addition.

Sample	Thickness (nm)	Maximum current density (mA/cm ²)
PANI – pH 5.9	6.30	0.028
PANI + SiO ₂ – pH 5.9	24.4	0.088
PANI + Au – pH 6.15	14.5	0.034
PANI – pH 3.9	38.2	0.099
PANI + SiO ₂ – pH 3.9	26.2	0.097
PANI – pH 1.5	185	0.963
PANI + SiO ₂ – pH 1.5	158	0.794

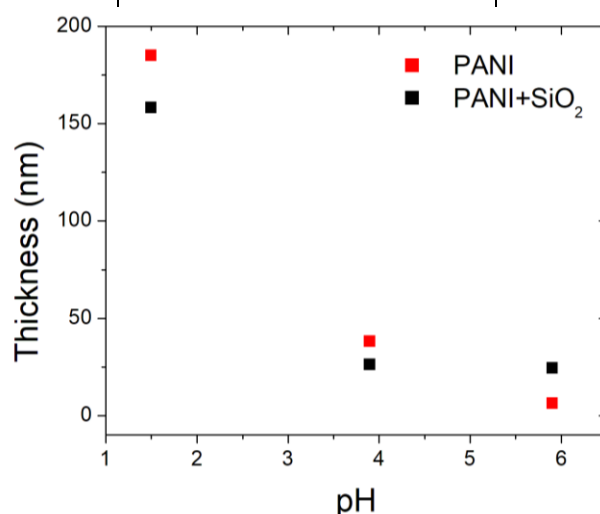


Figure 6. Thickness dependence on electrodeposition pH and influence of SiO₂ nanoparticles on thickness at different pH.

3.5. Atomic force microscopy.

AFM was performed in order to obtain film thickness. Table 2 presents the obtained AFM results and the maximum current density developed in cyclic voltammetry tests for comparison.

The decrease in film thickness and current density with increasing pH, well visualized in Figure 6, occurs because films obtained at less acid pH are composed of non-conducting pernigraniline [37,59], which diminishes the charge transfer between anode and solution in as much as the film grows. By adding SiO₂ nanoparticles, the reduction of thickness with increasing pH is also observed. However, when we compare the influence of nanoparticles at a determined pH, we observe an interesting fact. At pH of 1.5 and 3.9, the addition of nanoparticles reduces the film thickness and current density compared to the same pH without nanoparticles, while at a pH of 5.9, the nanoparticles have the opposite effect. Thus, the nanoparticle effect at pH 1.5 and 3.9 can be ascribed to nanoparticle screening, as will be discussed in the next section.

4. Discussion

In this work, physical effects refer to charge transfer and heterojunctions formation, while the chemical effects will be ascribed to the induction of changes in PANI oxidation states. As presented elsewhere [36], at pH 5.9 TiO₂ nanoparticles incorporated in PANI films have physical and chemical effects on films formation and its electric properties, that is: (i) TiO₂ nanoparticles act as a catalyst in the deposition process, promoting the formation of emeraldine instead of expected pernigraniline form of PANI; (ii) the interaction between PANI and TiO₂ nanoparticles, which is not screened at this pH, results in charge transfer and formation of a metallic heterojunction. In the case of SiO₂ and Au nanoparticles, the employed characterizations (UV-Vis and Raman) do not indicate any change in oxidation state, which allow us to discharge the chemical effects of these nanoparticles at pH 5.9 and 6.15 and to conclude that chemical effects of nanoparticles on deposited PANI film depend on the nanoparticles composition.

On the other hand, at pH of 5.9 and 6.15, cyclic voltammetry curves and AFM measurements (see Table 2) show an increase in current density and film thickness because of the presence of SiO₂ and Au nanoparticles. Similar to TiO₂ nanoparticles, SiO₂ and Au nanoparticles may transfer charge to the deposited PANI films they are in. Thus, in analogy as dopant atoms in a semiconductor, these nanoparticles could provide filled electron levels near the film conduction band or empty levels near the film valence band, intensifying the current density developed in cyclic voltammetry tests.

The scenario is quite different for a pH of 1.5 and 3.9. For the same pH, the presence of SiO₂ nanoparticles leads to a decrease in film thickness and currents (see Figure 6 and Table 2). Such results can be understood if one considers that SiO₂ nanoparticles around 10 nm, similar to those employed in this work, become positively charged for pH ≤ 4 [60]. Therefore, they are screened by the SO₄⁻² anions available in the solution before being incorporated in the film (as it is depicted in the top panel of Figure 7). Due to the screening of nanoparticles, fewer ions are available in the electropolymerization process, and, consequently, a small reduction in film thickness and current density is expected. Also, the screening of nanoparticles avoids the physical contact between nanoparticles and molecules of the film, which prevents any doping effect of the nanoparticles on the film that could contribute to increasing the current density.

Another evidence for the screening mechanism described above comes from the presence of S peaks in the EDS spectra. As mentioned earlier in the text, the only possible source of S atoms is the SO_4^{2-} anions originating from the electrolyte solution. The charge neutrality of the films demands compensation for SO_4^{2-} anions presence, which comes from the incorporated SiO_2 nanoparticles that are positively charged in solutions with $\text{pH} \leq 4$. In addition, the availability of SO_4^{2-} anions increases with decreasing pH, and the screening is, therefore, more effective for pH 1.5 than it is for 3.9, which explains why the S peak of Fig. 2 (a) is more intense than that of Fig. 2 (b). As previously reported, PANI films with TiO_2 incorporation also present S peaks for low pH, which also gives evidence for nanoparticle screening by SO_4^{2-} anions. Au nanoparticles can also be positively charged and screened by anions depending on the surrounding media [61,62]. In fact, a zeta potential analysis Au nanoparticles, whose size is very similar to that of nanoparticles used in work, indicates that they become positively charged for $\text{pH} \leq 4.6$ [63]. Therefore, similar to SiO_2 and TiO_2 nanoparticles, Au nanoparticles should also be screened by anions, which explain the absence of physical effects at low pH.

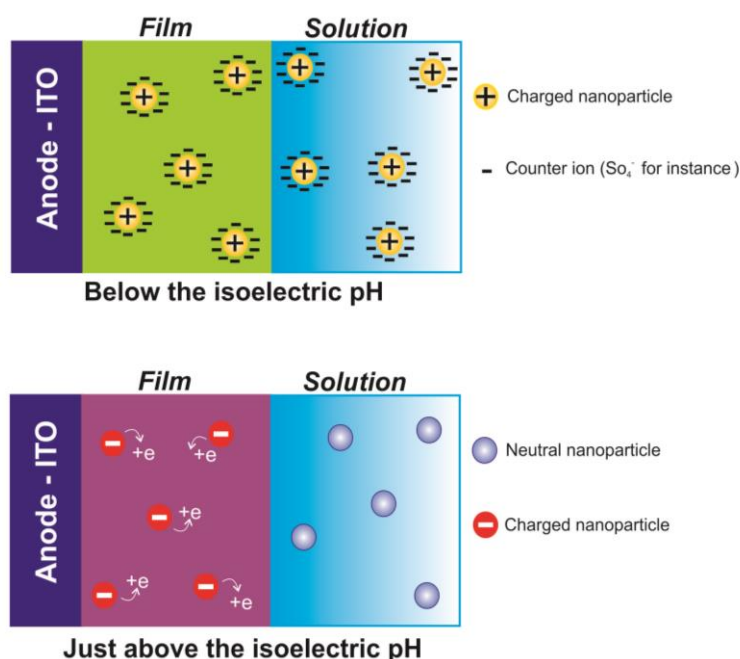


Figure 7. Below the isoelectric pH (top panel), the nanoparticles become positively charged and are screened by solution anions. The screened nanoparticles do not play any role in film properties. Above the isoelectric pH the screening mechanism becomes less effective as the pH approaches 7 because of the smaller amount of ions (H^+ and SO_4^{2-}) available in the solution, and nanoparticles are neutral (bottom panel) or negatively charged (not shown). When incorporated in the semiconducting film, the nanoparticles can act as dopants improving their conductivity. The depiction of nanoparticles as electron acceptors in the bottom panel is only illustrative as they could also be electron donors.

5. Conclusions

In summary, we have performed electropolymerization of pristine and hybrid PANI films at different pH. Unlike TiO_2 nanoparticles, SiO_2 and Au nanoparticles do not change the chemical properties (e.g., pernigraniline to emeraldine) of electrodeposited PANI films, which show that the chemical effects of nanoparticles incorporation on films is dependent on the nanoparticle composition. On the other hand, all mentioned nanoparticles improve the PANI film conductivity when incorporated at pH 5.9 and 6.15, suggesting a general physical effect. We ascribe such an effect on the ability of nanoparticles to dope the PANI films with electrons

or holes. This effect does not occur when the nanoparticles are incorporated at lower pH (1.5 and 3.9). To explain the presence/absence of physical and chemical effects of nanoparticles at different pH, we propose a mechanism based on the screening of charged nanoparticles supported by different experimental techniques.

Funding

Authors acknowledge financial support from CNPq, FAPEMIG, CAPES, PROPP/UFOP, and L'Oréal/UNESCO/ABC.

Acknowledgments

Authors acknowledge financial support from CNPq, FAPEMIG, CAPES, PROPP/UFOP, and L'Oréal/UNESCO/ABC. The authors also thank LCPNano (UFMG) for the Raman measurements and Nanolab (UFOP) for the SEM and EDS analysis.

Conflicts of Interest

The authors declare that they have no known competing financial interests or personal relationships that could have influenced the work reported in this paper.

References

1. Mattoso, L.H.C; MacDiarmid, A.G. Oxidation States of Polyanilines. *The Polymeric Materials Encyclopedia* **1996**, CRC.
2. Bhadra, J.; Alkareem, A.; Al-Thani, N. A review of advances in the preparation and application of polyaniline based thermoset blends and composites. *Journal of Polymer Research* **2020**, *27*, 122-142, <https://doi.org/10.1007/s10965-020-02052-1>.
3. Beygisangchin, M.; Rashid, S.A.; Shafie, S.; Sadrolhosseini, A.S.; Lim, H.N. Preparations, Properties, and Applications of Polyaniline and Polyaniline Thin Films—A Review. *Polymers* **2021**, *13*, 2003-2049, <https://doi.org/10.3390/polym13122003>.
4. Chandrakanthi, N.; Careem, M. Thermal stability of polyaniline. *Polymer Bulletin* **2000**, *44*, 101–108, <https://doi.org/10.1007/s002890050579>.
5. K, N.; Rout, C.S. Conducting polymers: a comprehensive review on recent advances in synthesis, properties and applications. *RSC Advances* **2021**, *11*, 5659-5697, <https://doi.org/10.1039/d0ra07800j>.
6. Bhadra, S.; Khastgir, D.; Singha, N.K.; Lee, J.H. Progress in Preparation, Processing and Applications of Polyaniline. *Progress in Polymer Science* **2009**, *34*, 783-810, <https://doi.org/10.1016/j.progpolymsci.2009.04.003>.
7. Sanches, E.A.; Soares, J.C.; Iost, R.M.; Marangoni, V.S.; Trovati, G.; Batista, T.; Mafud, A.C.; Zucolotto, V.; Mascarenhas, Y.P. Structural Characterization of Emeraldine-Salt Polyaniline/Gold Nanoparticles Complexes. *Journal of Nanomaterials* **2011**, 697071, <https://doi.org/10.1155/2011/697071>.
8. Okamoto, H.; Kotaka, T. Structure and properties of polyaniline films prepared via electrochemical polymerization. I: Effect of pH in electrochemical polymerization media on the primary structure and acid dissociation constant of product polyaniline films. *Polymer* **1998**, *39*, 4349-4358, [https://doi.org/10.1016/S0032-3861\(98\)00013-5](https://doi.org/10.1016/S0032-3861(98)00013-5).
9. Yoshioka, N.A.; Rocha, H.L.; Cazati, T.; Manhabosco, T.M.; Muller, I.L. Pulsed Electrodeposition of Polyaniline Films used as Photogenerated Charge Transporting Layers in Organic Photovoltaic Devices. *Polimeros* **2014**, *24*, 88-93, <https://doi.org/10.4322/polimeros.2013.061>.
10. Ates, M.; Serin, M.A.; Ekmen, I.; Ertas, Y.N. Supercapacitor behaviors of polyaniline/CuO, polypyrrole/CuO and PEDOT/CuO nanocomposites. *Polymer Bulletin* **2015**, *72*, 2573-2589, <https://doi.org/10.1007/s00289-015-1422-4>.

11. Al-Haidary, Q.N.; Al-Mokaram, A.M.; Hussein, F.M.; Ismail, A.H. Development of polyaniline for sensor applications: A review. *Journal of Physics: Conference Series* **2020**, *1853*, 012062, <https://doi.org/10.1088/1742-6596/1853/1/012062>.
12. Gómez, I.J.; Sulleiro, M.V.; Mantione, D.; Alegret, N. Carbon Nanomaterials Embedded in Conductive Polymers: A State of the Art. *Polymers* **2021**, *13*, 745, <https://doi.org/10.3390/polym13050745>.
13. Xu, K.; Zhang, Q.; Hao, Z.; Tang, Y.; Wang, H.; Liu, J.; Yan, H. Integrated electrochromic supercapacitors with visual energy levels boosted by coating onto carbon nanotube conductive networks. *Solar Energy Materials and Solar Cells* **2020**, *206*, 110330, <https://doi.org/10.1016/j.solmat.2019.110330>.
14. Ben, J.; Song, Z.; Liu, X.; Lü, W.; Li, X. Fabrication and Electrochemical Performance of PVA/CNT/PANI Flexible Films as Electrodes for Supercapacitors. *Nanoscale Research Letters* **2020**, *15*, 151, <https://doi.org/10.1186/s11671-020-03379-w>.
15. Kazemi, F.; Naghib, S.M.; Zare, Y.; Rhee, K.Y. Biosensing Applications of Polyaniline (PANI)- Based Nanocomposites: A Review. *Polymer Reviews* **2020**, 1-45, <https://doi.org/10.1080/15583724.2020.1858871>.
16. Brachetti-Sibaja, S.B.; Palma-Ramírez, D.; Torres-Huerta, A.M.; Domínguez-Menezes, M.A.; Dorantes-Rosales, H.J.; Rodríguez-Salazar, A.E.; Ramírez-Meneses, E. CVD Conditions for MWCNTs Production and Their Effects on the Optical and Electrical Properties of PPy/MWCNTs, PANI/MWCNTs Nanocomposites by In Situ Electropolymerization. *Polymers* **2021**, *13*, 351, <https://doi.org/10.3390/polym13030351>.
17. Jangid, N.K.; Jadoun, S.; Kaur, N. A review on high-throughput synthesis, deposition of thin films and properties of polyaniline. *European Polymer Journal* **2020**, *15*, 109485, <https://doi.org/10.1016/j.eurpolymj.2020.109485>.
18. Kim, J.Y.; Iqbal, S.; Jang, H.J.; Jung, E.Y.; Bae, G.T.; Park, C-S.; Tae, H-S. In-Situ Iodine Doping Characteristics of Conductive Polyaniline Film Polymerized by Low-Voltage-Driven Atmospheric Pressure Plasma. *Polymers* **2021**, *13*, 418, <https://doi.org/10.3390/polym13030418>.
19. Charoensri, K.; Rodwihok, C. Wongratanaphisan, D.; Ko, J.A.; Chung, J.S.; Park, H.J. Investigation of Functionalized Surface Charges of Thermoplastic Starch/Zinc Oxide Nanocomposite Films Using Polyaniline: The Potential of Improved Antibacterial Properties. *Polymers* **2021**, *13*, 425, <https://doi.org/10.3390/polym13030425>.
20. Lyu, H. Triple Layer Tungsten Trioxide, Graphene, and Polyaniline Composite Films for Combined Energy Storage and Electrochromic Applications. *Polymers* **2020**, *12*, 49, <https://doi.org/10.3390/polym12010049>.
21. Ramanavicius, S.; Ramanavicius, A. Conducting Polymers in the Design of Biosensors and Biofuel Cells. *Polymers* **2021**, *13*, 49, <https://doi.org/10.3390/polym13010049>.
22. Iqbal, J.; Ansani, M.O.; Numan, A.; Wageh, S.; Al-Ghamdi, A.; Alam, M.G.; Kumar, P.; Jafer, R.; Bashir, S.; Rajpar, A.H. Hydrothermally Assisted Synthesis of Porous Polyaniline@Carbon Nanotubes–Manganese Dioxide Ternary Composite for Potential Application in Supercapattery. *Polymers* **2020**, *12*, 2918, <https://doi.org/10.3390/polym12122918>.
23. Ghorbani, F.; Zamanian, A.; Aidun, A. Conductive Electrospun Polyurethane-Polyaniline Scaffolds Coated with Poly(vinyl alcohol)-GPTMS under Oxygen Plasma Surface Modification. *Materials Today Communications* **2020**, *22*, 100752, <https://doi.org/10.1016/j.mtcomm.2019.100752>.
24. Zare, E.N.; Makvandi, P.; Ashtari, B.; Rossi, F.; Motahari, A.; Perale, G. Progress in Conductive Polyaniline-Based Nanocomposites for Biomedical Applications: A Review. *Journal of Medicinal Chemistry* **2020**, *63*, 1-22, <https://doi.org/10.1021/acs.jmedchem.9b00803>.
25. Bejbouji, H.; Vignau, L.; Miane, J.L.; Dang, M-T.; Oualim, E.M.; Harmouchi, M.; Mouhsen, A. Polyaniline as a hole injection layer on organic photovoltaic cells. *Solar Energy Materials and Solar Cells* **2010**, *94*, 176-181, <https://doi.org/10.1016/j.solmat.2009.08.018>.
26. Liu, Z.; Zhou, J.; Xué, H.; Shen, L.; Zang, H.; Chen, W. Polyaniline/TiO₂ solar cells. *Synthetic Metals* **2006**, *156*, 721-723, <https://doi.org/10.1016/j.synthmet.2006.04.001>.
27. Pandey, P.; Singh, S.P.; Arya, S.K.; Sharma, A.; Datta, M.; Malhotra, B.D. Gold Nanoparticles-Polyaniline Composite Films for Glucose Sensing. *Journal of Nanoscience and Nanotechnology* **2008**, *8*, 1-6, <https://doi.org/10.1166/jnn.2008.349>.
28. German, N.; Ramanaviciene, A.; Ramanavivius, A. Dispersed Conducting Polymer Nanocomposites with Glucose Oxidase and Gold Nanoparticles for the Design of Enzymatic Glucose Biosensors. *Polymers* **2021**, *13*, 2173, <https://doi.org/10.3390/polym13132173>.
29. Zubillaga, O.; Cano, F.J.; Azkarate, I.; Molchan, I.S.; Thompson, G.E.; Skeldon, P. Anodic Films Containing Polyaniline and Nanoparticles for Corrosion Protection of AA2024T3 Aluminium Alloy. *Surface and Coatings Technology* **2009**, *203*, 1494-1501, <https://doi.org/10.1016/j.surfcoat.2008.11.023>.

30. Choudhury, A. Polyaniline/Silver Nanocomposites: Dielectric Properties and Ethanol Vapour Sensitivity. *Sensor and Actuators B Chemical* **2009**, *138*, 318-325, <https://doi.org/10.1016/j.snb.2009.01.019>.
31. Manhabosco, T.M.; Mueller, I.L. Deposition of thin cobalt films onto silicon by galvanostatic and potentiostatic techniques. *Journal of Materials Science* **2009**, *44*, 2931-2937, <https://doi.org/10.1007/s10853-009-3388-9>.
32. Manhabosco, T.M.; Martins, L.A.M.; Tamborim, S.M.; Ilha, M.; Vieira, M.Q.; Guma, F.C.R.; Müller, I.L. Cell response and corrosion behavior of electrodeposited diamond-like carbon films on nanostructured titanium. *Corrosion Science* **2013**, *66*, 169-176, <https://doi.org/10.1016/j.corsci.2012.09.015>.
33. Manhabosco, T.M.; Muller, I.L. Electrodeposition of diamond-like carbon (DLC) films on Ti. *Applied Surface Science* **2009**, *255*, 4082-4086, <https://doi.org/10.1016/j.apsusc.2008.10.087>.
34. Manhabosco, T.M.; Aloni, S.; Kuykendall, T.R.; Manhabosco, S.M.; Batista, A.B.; Soares, J.S.; Barboza, A.P.M.; Oliveira, A.B.; Batista, R.J.C.; Urban, J.J. Electrochemical Atomic Layer Epitaxy Deposition of Ultrathin SnTe Films. *Recent Progress in Materials* **2019**, *1*, 12, <https://doi.org/10.21926/rpm.1904005>.
35. Zheng, H.; Liu, M.; Yan, Z.; Chen, J. Highly selective and stable glucose biosensor based on incorporation of platinum nanoparticles into polyaniline-montmorillonite hybrid composites. *Microchemical Journal* **2020**, *152*, 104266, <https://doi.org/10.1016/j.microc.2019.104266>.
36. Filho, V.F.L.; Machado, G.; Batista, R.J.C.; Soares, J.S.; Oliveira, A.B.; Vasconcelos, C.; Lino, A.A.; Manhabosco, T.M. Effect of TiO₂ nanoparticles on polyaniline films electropolymerized at different pH. *The Journal of Physical Chemistry C* **2016**, *120*, 27, 14977-14983, <https://doi.org/10.1021/acs.jpcc.6b04919>.
37. Piella, J.; Bastús, N.G.; Puntès, V. Size-controlled Synthesis of sub-10 nm Citrate-stabilized Gold Nanoparticles and Related Optical Properties. *Chemistry of Materials* **2016**, *28*, 1066-1075, <https://doi.org/10.1021/acs.chemmater.5b04406>.
38. Stejskal, J.; Kratochvíl, P.; Radhakrishnan, N. Polyaniline dispersions 2. UV-Vis absorption spectra. *Synthetic Metals* **1993**, *61*, 225-231, [https://doi.org/10.1016/0379-6779\(93\)91266-5](https://doi.org/10.1016/0379-6779(93)91266-5).
39. Goswami, S.; Nandy, S.; Calmeiro, T.R.; Igreja, R.; Martins, R.; Fortunato, E. Stress induced mechano-electrical writing-reading of polymer film powered by contact electrification mechanism. *Scientific Reports* **2016**, *6*, 19514, <https://doi.org/10.1038/srep19514>.
40. Lee, J.Y.; Su, X.H.; Qui, C.Q. Characterization of electrodeposited copolymers of aniline and metanilic acid. *Journal of Electroanalytical Chemistry* **1994**, *367*, 71-78, [https://doi.org/10.1016/0022-0728\(93\)03014-G](https://doi.org/10.1016/0022-0728(93)03014-G).
41. Abdiryim, T.; Xiao-Gang, Z.; Jamal, R. Comparative studies of solid-state synthesized polyaniline doped with inorganic acids. *Materials Chemistry and Physics* **2005**, *90*, 367-372, <https://doi.org/10.1016/j.matchemphys.2004.10.036>.
42. Albuquerque, J.E.; Mattoso, L.H.C.; Faria, R.M.; Masters, J.G.; MacDiarmid, A.G. Study of the interconversion of polyaniline oxidation states by optical absorption spectroscopy. *Synthetic Metals* **2004**, *146*, 1-10, <https://doi.org/10.1016/j.synthmet.2004.05.019>.
43. Albuquerque, J.E.; Mattoso, L.H.C.; Balogh, D.T.; Faria, R.M.; Masters, J.G.; MacDiarmid, A.G. A simple method to estimate the oxidation state of polyanilines. *Synthetic Metals* **2000**, *133*, 19-22, [https://doi.org/10.1016/S0379-6779\(99\)00299-4](https://doi.org/10.1016/S0379-6779(99)00299-4).
44. Bocchini, S.; Chiolerio, A.; Porro, S.; Accardo, D.; Garino, N.; Bejtka, K.; Perrone, D.; Pirri, C.F. Synthesis of polyaniline-based inks, doping thereof and test device printing towards electronic applications. *Journal of Materials Chemistry C* **2013**, *1*, 5101-5109, <https://doi.org/10.1039/C3TC30764F>.
45. Nabid, M.R.; Golbabaee, M.; Moghaddam, A.B.; Dinarvand, R.; Sedghi, R. Polyaniline/TiO₂ nanocomposite: enzymatic synthesis and electrochemical properties. *International Journal of Electrochemical Science* **2008**, *3*, 1117-1126.
46. Yoon, S-B.; Yoon, E-H.; Kim, K-B. Electrochemical properties of leucoesmeraldine, emeraldine and pernigraniline forms of polyaniline/multi-wall carbon nanotube nanocomposites for supercapacitor applications. *Journal of Power Sources* **2011**, *196*, 10791-10797, <https://doi.org/10.1016/j.jpowsour.2011.08.107>.
47. Lindfors, T.; Kvarnström, C.; Ivaska, A. Raman and UV-Vis spectroscopic study of polyaniline membranes containing a bulk cationic additive. *Journal of Electroanalytical Chemistry* **2002**, *518*, 131-138, [https://doi.org/10.1016/S0022-0728\(01\)00704-5](https://doi.org/10.1016/S0022-0728(01)00704-5).
48. Lindfors, T.; Ivaska, A. pH sensitivity of polyaniline and its substituted derivatives. *Journal of Electroanalytical Chemistry* **2002**, *531*, 43-52, [https://doi.org/10.1016/S0022-0728\(02\)01005-7](https://doi.org/10.1016/S0022-0728(02)01005-7).
49. Weng, S.; Lin, Z.; Chen, L.; Zhou, J. Electrochemical synthesis and optical properties of helical polyaniline nanofibers. *Electrochimica Acta* **2010**, *55*, 2727-2733, <https://doi.org/10.1016/j.electacta.2009.12.032>.

50. Vivekanandan, J.; Ponnusamy, V.; Mahudewaran, A.; Vijayanand, P.S. Synthesis, characterization and conductivity study of polyaniline prepared by chemical oxidative and electrochemical methods. *Archives of Applied Science Research* **2011**, *3*, 147-153.
51. Jaramillo-Tabares, B.E.; Isaza, F.J.; Torresi, S.I.C. Stabilization of polyaniline by the incorporation of magnetite nanoparticles. *Materials Chemistry and Physics* **2012**, *132*, 529-533, <https://doi.org/10.1016/j.matchemphys.2011.11.065>.
52. Masters, J.G.; Sun, Y.; MacDiarmid, A.G.; Epstein, A.J. Polyaniline: allowed oxidation states. *Synthetic Metals* **1991**, *41*, 715-718, [https://doi.org/10.1016/0379-6779\(91\)91166-8](https://doi.org/10.1016/0379-6779(91)91166-8).
53. Passeri, D.; Tamburri, E.; Terranova, M.L.; Rossi, M. Polyaniline-nanodiamond fibers resulting from the self-assembly of nano-fibrils: a nanomechanical study. *Nanoscale* **2015**, *7*, 14358-14367, <https://doi.org/10.1039/C5NR02096D>.
54. Jain, M.; Annapoorni, S. Raman study of polyaniline nanofibers prepared by interfacial polymerization. *Synthetic Metals* **2010**, *160*, 1727-1732, <https://doi.org/10.1016/j.synthmet.2010.06.008>.
55. Mazeikiene, R.; Statino, A.; Kuodis, Z.; Niaura, G.; Malinauskas, A. *In situ* Raman spectroelectrochemical study of self-doped polyaniline degradation kinetics. *Electrochemistry Communications* **2006**, *8*, 1082-1086, <https://doi.org/10.1016/j.elecom.2006.04.017>.
56. Bernard, M.C.; Cordoba-Torresi, S.; Goff, A.H-L. Electrochromic phenomena in polyaniline films. Effect of pH and influence of the sweep range on cycling lifetimes studied by *in situ* Raman spectroscopy. *Solar Energy Materials and Solar Cells* **1992**, *25*, 225-240, [https://doi.org/10.1016/0927-0248\(92\)90070-6](https://doi.org/10.1016/0927-0248(92)90070-6).
57. Arsov, L.D.; Plieth, W.; Kobmehl, G. Electrochemical and Raman spectroscopic study of polyaniline; influence of the potential on the degradation of polyaniline. *Journal of Solid State Electrochemistry* **1998**, *2*, 355-361, <https://doi.org/10.1007/s100080050112>.
58. Trchová, M.; Konyushenko, E.N.; Stejskal, J.; Kovářová, J.; Ćirić-Marjanović, G. The conversion of polyaniline nanotubes to nitrogen-containing carbon nanotubes and their comparison with multi-walled carbon nanotubes. *Polymer Degradation and Stability* **2009**, *94*, 929-938, <https://doi.org/10.1016/j.polymdegradstab.2009.03.001>.
59. Obaid, A.Y.; El-Mossalamy, E.H.; Al-Thabaiti, S.A.; El-Hallag, I.S.; Hermas, A.A.; Asiri, A.M. Electrodeposition and Characterization of Polyaniline on Stainless Steel Surface via Cyclic, Convulsive Voltammetry and SEM in Aqueous Acidic Solutions. *International Journal of Electrochemical Science* **2014**, *9*, 1003-1015.
60. Liu, Q.; Sun, Z.; Santamarina, J.C. Transport and Adsorption of Silica Nanoparticles in Carbonate Reservoirs: A Sand Column Study, *Energy Fuels* **2019**, *33*, 4009-4016, <https://doi.org/10.1021/acs.energyfuels.9b00057>.
61. Martins, J.R.; Batista, R.J.C.; Chacham, H. Doped assemblies of gold nanoparticles: Structural and Electronic properties. *Journal of the American Chemical Society* **2010**, *132*, 11929-11933, <https://doi.org/10.1021/ja910335h>.
62. Batista, R.J.C.; Mazzoni, M.S.C.; Chacham, H. First-principles investigation of electrochemical properties of gold nanoparticles. *Nanotechnology* **2010**, *21*, 065705, <https://doi.org/10.1088/0957-4484/21/6/065705>.
63. Brewer, S.H.; Glomm, W.R.; Johnson, M.C.; Knag, M.K.; Franzen, S. Probing BSA Binding to Citrate-Coated Gold Nanoparticles and Surfaces. *Langmuir* **2005**, *21*, 9303-9307, <https://doi.org/10.1021/la050588t>.